The performance limits of epigraphene Hall sensors doped across the Dirac point

Applied Physics Letters

The performance limits of epigraphene Hall sensors doped across the Dirac point

Cite as: Appl. Phys. Lett. **116**, 223504 (2020); https://doi.org/10.1063/5.0006749
Submitted: 05 March 2020 . Accepted: 19 May 2020 . Published Online: 01 June 2020

H. He, N. Shetty, T. Bauch, S. Kubatkin, T. Kaufmann, M. Cornils, R. Yakimova, and S. Lara-Avila

Applied Physics Letters ARTICLE scitation.org/journal/apl

The performance limits of epigraphene Hall sensors doped across the Dirac point

Cite as: Appl. Phys. Lett. **116**, 223504 (2020); doi: 10.1063/5.0006749
Submitted: 5 March 2020 · Accepted: 19 May 2020 ·
Published Online: 1 June 2020

H. He,[1,a] N. Shetty,[1] T. Bauch,[1] S. Kubatkin,[1] T. Kaufmann,[2] M. Cornils,[2] R. Yakimova,[3] and S. Lara-Avila[1,4]

AFFILIATIONS

[1]Department of Microtechnology and Nanoscience, Chalmers University of Technology, 412 96 Gothenburg, Sweden
[2]TDK-Micronas GmbH, Hans-Bunte-Strasse 19, D-79108 Freiburg, Germany
[3]Department of Physics, Chemistry and Biology, Linkoping University, 581 83 Linköping, Sweden
[4]National Physical Laboratory, Hampton Road, Teddington TW11 0LW, United Kingdom

[a]Author to whom correspondence should be addressed: hanshe@chalmers.se

ABSTRACT

Epitaxial graphene on silicon carbide, or epigraphene, provides an excellent platform for Hall sensing devices in terms of both high electrical quality and scalability. However, the challenge in controlling its carrier density has thus far prevented systematic studies of epigraphene Hall sensor performance. In this work, we investigate epigraphene Hall sensors where epigraphene is doped across the Dirac point using molecular doping. Depending on the carrier density, molecular-doped epigraphene Hall sensors reach room temperature sensitivities of $S_V = 0.23$ V/(VT) and $S_I = 1440$ V/(AT), with magnetic field detection limits down to $B_{MIN} = 27$ nT/$\sqrt{\text{Hz}}$ at 20 kHz. Thermally stabilized devices demonstrate operation up to 150 °C with $S_V = 0.12$ V/(VT), $S_I = 300$ V/(AT), and $B_{MIN} \sim 100$ nT/$\sqrt{\text{Hz}}$ at 20 kHz. Our work demonstrates that epigraphene doped close to the Dirac point could potentially outperform III–V Hall elements in the extended and military temperature ranges.

Based on the classical Hall effect, solid-state Hall sensors represent a large portion of magnetometers, which are extensively used in automotive, marine, and consumer electronics applications. Hall sensors based on silicon have a widespread use owing to well-established and low-cost production methods,[1–3] but increasing requirements placed on improved magnetic performance or resilience to harsh conditions like high temperatures demand the exploration of other even more suitable materials.[4]

Hall sensors detect magnetic fields by measuring the Hall voltage V_H induced by an external field B. High device sensitivity implies a large magnitude of V_H response to an external field, for a given bias current I_B or voltage V_B. This leads to two important material-related metrics: the current-related sensitivity $S_I = \left|V_H/(BI_B)\right|$ [V/(AT)], which is essentially determined by the Hall coefficient R_H (Ω/T), and the voltage-related sensitivity $S_V = \left|V_H/(BV_B)\right|$ [V/(VT)], which is ultimately limited by the carrier mobility $\mu = R_H/\rho$ [m^2/(V s)], where ρ is the sheet resistance.

Graphene appears to be a natural candidate for highly sensitive Hall elements due to its high mobility and the possibility to tune carrier density n toward charge neutrality (Dirac point). Low carrier density is desirable because it increases the Hall coefficient, $R_H = 1/(ne)$.[5,6] Moreover, since the mobility $\mu = R_H/\rho$ of graphene is inversely proportional to carrier density as $\mu \propto 1/\sqrt{n}$,[7] decreasing n toward neutrality would increase both S_I and S_V. In principle, low n leads to an increase in ρ, which follows the relation $\rho \propto 1/n$, in the limit where charged impurity scattering dominates (supplementary material S1).[8,9] Yet, decreasing n can actually lead to a lower magnetic field detection limit, $B_{MIN} = V_N/(\mathrm{I_B R_H})$ (T/$\sqrt{\text{Hz}}$), where V_N is the voltage noise spectral density (V/$\sqrt{\text{Hz}}$). If Johnson–Nyquist noise dominates, then $V_N = V_{TH} \propto \sqrt{4k_BT\rho}$, with k_B being the Boltzmann constant, T the temperature, and the detection limit scaling as $B_{MIN} \propto V_N/\mathrm{R_H} \propto \sqrt{n}$ for a fixed I_B. Disorder in real graphene samples prevents it from reaching true charge neutrality, but high-quality graphene can approach low carrier densities $n \sim 10^{10}$ cm^{-2} at cryogenic temperatures.[10,11]

The highest-quality graphene is obtained by mechanical exfoliation of graphite and encapsulation in hexagonal boron nitride (hBN-G). As a Hall sensor, hBN-G has shown ultra-high device sensitivities and detection limits comparable to those of silicon.[12] However, this approach serves only as a proof-of-principle of the capabilities of graphene Hall sensors since device fabrication cannot be scaled up. Graphene grown using chemical vapor deposition (CVD) is a more

scalable technology, which can also reach high sensitivities, but reported performance varies greatly,[13–15] perhaps due to variability in material growth and the need for subsequent transfer to suitable substrates.[16]

Epitaxial graphene on the SiC substrate (epigraphene) is another attractive scalable technology. The insulating substrate allows for direct mass fabrication of devices over wafer scales,[17,18] forgoing the need for graphene transfer, thus increasing reproducibility and yield. Epigraphene is also compatible with operation at temperatures exceeding common industrial requirements.[19,20] Despite these advantages, epigraphene remains relatively unexplored for Hall sensing in the literature, possibly owing to the difficulties in tuning carrier density due to high intrinsic n-doping, pinned by the substrate.[21–23]

We report the exploration of the performance limits of epigraphene Hall sensors for varying doping levels across the Dirac point. Carrier density control is enabled by a molecular doping method using electron acceptors F4TCNQ assembled on the surface of epigraphene.[11] Devices doped using this method have already shown excellent electrical properties and low charge disorder, albeit at low temperatures.[24,25] We investigate Hall sensor figures of merit B_{MIN}, S_V, S_I, and finally thermal stability in ambient conditions from room temperature and just above 200 °C. Furthermore, we establish the limits for optimal operation of epigraphene Hall devices under realistic operational conditions.

Epigraphene was grown on 4H-SiC chips encased in a graphite crucible and heated using RF heating to around 1850 °C in an inert atmosphere of 1 bar argon.[17] Transmission mode microscopy was used to select only samples with over 90% monolayer coverage.[26] Device fabrication was performed using standard electron beam lithography. Epigraphene was removed using oxygen plasma etching, and the metal contacts were deposited using physical vapor deposition of 5 nm Ti and 80 nm Au. The finished device was spin coated with molecular dopants and the final carrier density was tuned by annealing at $T = 160$ °C, with varying annealing times depending on the desired final doping level.[11] Electrical characterization was performed primarily using the Van der Pauw (VdP) method, with samples measured at room temperature and under ambient conditions unless otherwise stated. A magnetic field perpendicular to the chip surface was applied using a coil electromagnet up to 100 mT. Noise measurements were performed by taking the power spectral density (PSD) using a voltage amplifier DLPVA-100-F-D from Femto Messtechnik GmbH, with the bandwidth limited to 100 kHz and the measured input noise level of 9 nV/√Hz. High-field measurements were performed using a PPMS (Physical Property Measurement System from Quantum Design) cryostat (2–300 K) with a superconducting magnet providing fields up to 14 T. For heating experiments, the sample was mounted using epoxy on a ceramic heater, and temperature was monitored using a Pt100-resistor.

Seven epigraphene Hall sensors [Fig. 1(a)], spread across four chips, were investigated in total. They were designed using symmetric square or cross-shaped geometries optimized with respect to S_V.[27,28] Cryogenic measurements on a molecular-doped sensor demonstrates a full transition to the half-integer Quantum Hall regime, with vanishing longitudinal resistance ρ_{XX} and quantized transverse resistance $R_{XY} = h/(2e^2)$ [Fig. 1(b)]. These measurements verify that the devices are made of high-quality monolayer graphene with uniform doping.

Hall measurements of the transverse resistance $R_{XY} = V_H/I_B$ serve as a basis for the evaluation of epigraphene Hall magnetometers. The Hall coefficient, carrier densities, and mobilities are calculated from measurements in low magnetic fields ($B < 0.5$ T) as $R_H = dR_{XY}/dB$, $n = 1/(eR_H)$, and $\mu = R_H/\rho$, respectively. For the low-field range, the linearity error of R_{XY} is below 1%, which is determined by the percentage deviation of the raw data from the low-field linear fit [Fig. 2(a)]. The samples were tested up to $B = 13$ T at room temperature. For low doping ($R_H = 1284\ \Omega$/T), the transversal resistance remains within 5% error in a range of $B = \pm 1.2$ T, but for higher doping ($R_H = 949\ \Omega$/T), the 5% error range increases to $B = \pm 6$ T. The non-linearity of R_{XY} is approximately $R_{XY} \propto B^2$ and is known to arise from geometrical and material correction effects.[29] Figure 2(b) shows a summary of the carrier densities achieved in our experiments. The gap in data near charge neutrality ($n = 0$) indicates the disordered charge-puddle regime, characterized by a highly non-linear low-field R_{XY}.[11] At room temperature, the maximum measured values of R_H and μ are $R_H = 1440\ \Omega$/T and $\mu = 2300\ \mathrm{cm^2/(V\,s)}$, respectively. In terms of charge disorder, at room temperature, epigraphene is in the puddle regime for doping levels $|n| < 5 \times 10^{11}\ \mathrm{cm^{-2}}$, thus setting the maximum R_H attainable in our epigraphene samples.

Figure 2(c) shows the linearity of V_H at 100 mT up to the bias current of 6 mA, measured for highly and lowly doped devices. We find that for all carrier densities, the current–voltage (I–V) characteristic is linear within 5% error for $I_B < 2.5$ mA. The non-linearity is expected to be

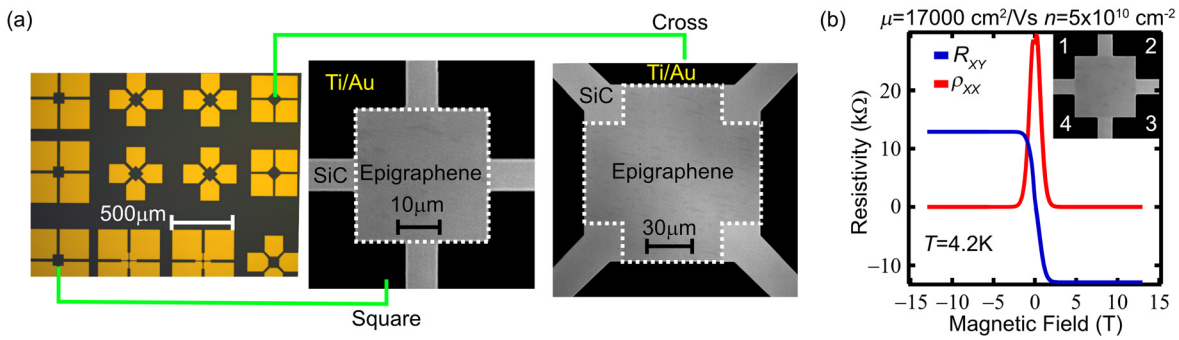

FIG. 1. (a) Optical micrographs of the layout of the investigated epigraphene Hall sensors. Each chip contains an array of sensors with square and cross-shaped geometries. (b) Molecular-doped Hall sensor displays the half-integer quantum Hall effect at cryogenic temperatures. R_{XY} used, e.g., contacts 1–3 for bias current and 2–4 to measure Hall voltage. ρ_{XX} used, e.g., 1–2 for bias and 4–3 for voltage measurements.

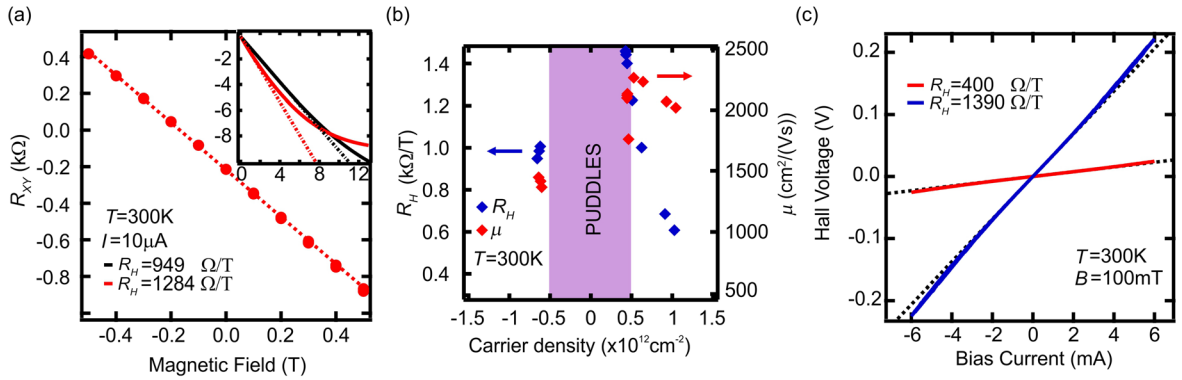

FIG. 2. (a) Hall measurements showing linearity of R_{XY} vs applied magnetic field. The inset shows behavior up to 13 T for different doping. The dotted lines are linear fits to low-field data $|B| < 0.5$ T. (b) Carrier densities n and mobilities μ are extracted from low-field Hall measurements. (c) Linearity of Hall voltage measured at a fixed field of 100 mT vs applied bias current for highly ($R_H = 400$ Ω/T; $n = 1.6 \times 10^{12}$ cm^{-2}) and lowly ($R_H = 1390$ Ω/T; $n = 4.5 \times 10^{11}$ cm^{-2}) doped devices. The dotted lines are linear fits to low-bias data $|I_B| < 0.5$ mA. The offset in V_H at zero field can be compensated by orthogonal vdP measurements and spinning current.[29] Typically observed offsets are on the order of 1 mV for a bias current of $I_B = 10$ μA (supplementary material S3).

ultimately due to self-heating. For instance, the measured Hall voltage may have a longitudinal voltage component, which can change non-linearly with a bias current due to Joule heating (supplementary material S2).[29–31] For all subsequent measurements, we limit the bias current to below 1.5 mA to ensure a linear I–V behavior within 2% error.

The measurements in magnetic fields are complemented with noise measurements to unveil the minimum detection limit B_{MIN}. Figure 3(a) shows the low-bias ($I_B = 10$ μA) voltage noise spectral density V_N measured at the Hall voltage terminals for different doping levels. In the low bias regime, the corner frequency of $1/f$ noise is around ∼30 Hz. As doping in epigraphene approaches the Dirac point, the sheet resistance of the devices increases as $\rho \propto 1/n$, and consequently, the larger input and output resistance of the devices increases thermal noise. Dotted lines in Fig. 3(a) are the thermal voltage noise V_{TH} calculated using measured input resistance. The agreement with experimental noise data points to the fact that, at low bias, thermal noise dominates in our sensors. Figure 3(b) shows the increase in the $1/f$ noise contribution at larger bias currents, which nearly follows Hooge's empirical relation [Fig. 3(b) inset],[32] implying that the excess noise is mostly due to resistance fluctuations. The Hooge parameter α_H, which is an indication of noisiness of the devices, is in the range of $\alpha_H \approx 10^{-5}$–10^{-4} for $n = 4.4 \times 10^{11}$–1.3×10^{12} cm^{-2}, lower than that of suspended graphene samples[33] and comparable to that of GaAs.[34] The deviation from ideal linear behavior could be due to joule heating[30] and carrier density excitations.[15] In practical devices, the excess noise can be alleviated by using spinning Hall current measurement techniques.[29]

The measured sensitivities for epigraphene Hall sensors and their dependence on doping, collected across all measured devices, are

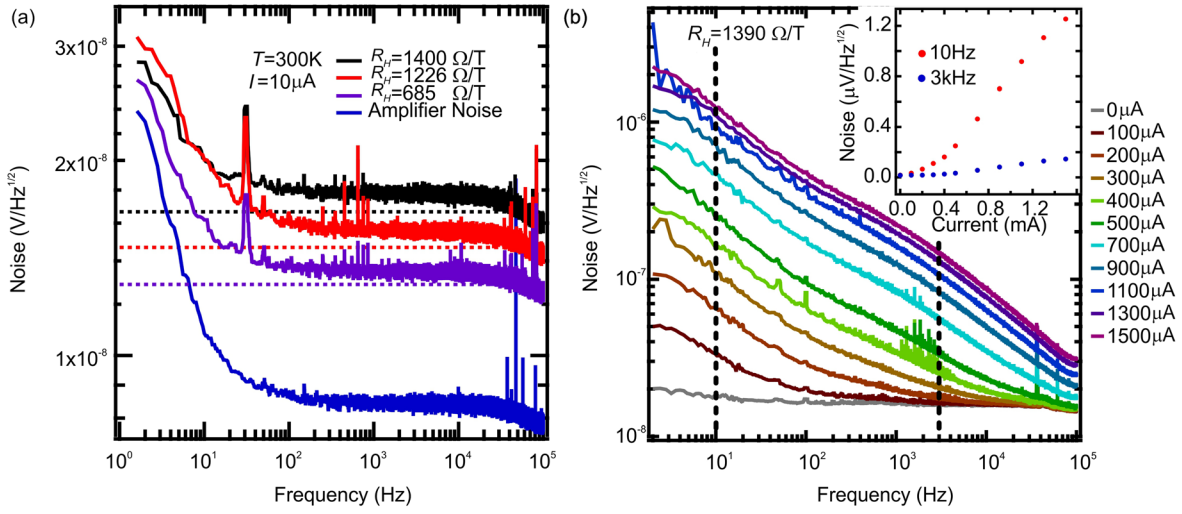

FIG. 3. (a) Noise performance for one Hall sensor measured at different doping levels. The dotted lines are calculated noise levels assuming pure thermal noise of a resistor. (b) Measured voltage noise spectral density vs bias current in another lowly doped device. Noise peaks related to the power line have been partially filtered out digitally with sliding window averaging. Inset: the noise amplitude vs bias current at two different frequencies (black dotted lines).

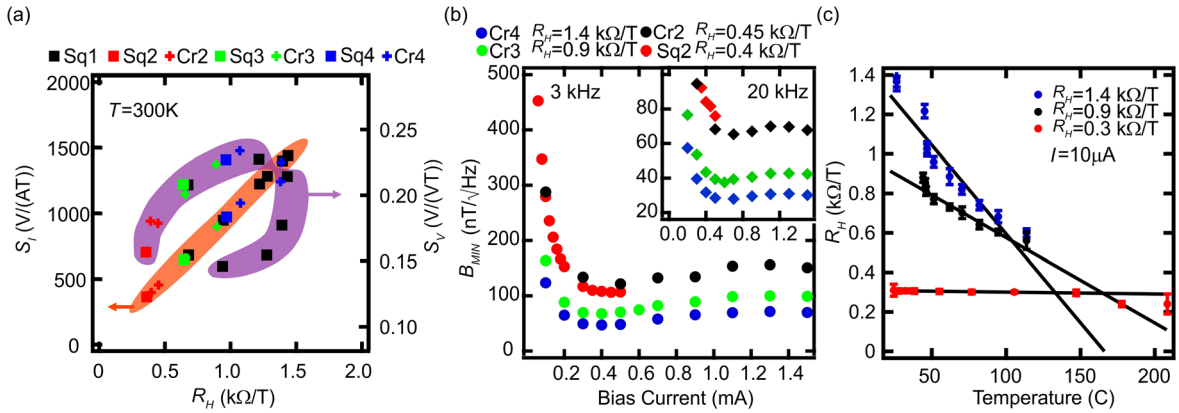

FIG. 4. (a) S_I (orange region) and S_V (purple region) vs R_H compiled from seven Hall sensors across four chips (Sq = square shaped; Cr = cross shaped). The two sequences of data points span high to low doping (starting from the leftmost point). (b) B_{MIN} vs bias current calculated directly from measured noise data for 3 kHz. The inset also shows data for 20 kHz. (c) Investigation of thermal stability of R_H by measuring R_H at elevated sample temperatures, for different initial room temperature doping. The error bars represent two standard deviations for measured R_H averaged over 10–15 min of measurements. Samples at low carrier density experience a permanent doping change at around 80 °C. But the cured device (red squares) is robust against thermal cycling up to 150 °C.

summarized in Fig. 4(a). The highest S_I is reached for low doping levels, close to the puddle regime $n \sim 5 \times 10^{11}$ cm^{-2}. The highest S_V occurs slightly outside the puddle regime, at doping levels $n \sim 6 \times 10^{11}$ cm^{-2}. We have performed full noise spectrum characterization [e.g., Fig. 3(b)] for four doping levels to obtain $B_{MIN} = V_N/(I_B R_H)$, which includes not only intrinsic noise of epigraphene (thermal and $1/f$ noise) but also amplifier noise. Figure 4(b) shows B_{MIN} as a function of I_B, measured at a frequency of 3 kHz for fair comparison to other graphene devices reported in the literature. The best B_{MIN} = 47 nT/√Hz is attained at lowest doping $n \sim 5 \times 10^{11}$ cm^{-2}, for $I_B = 400$ μA. At higher frequencies, where the $1/f$ noise contribution is lower, B_{MIN} can be naturally lower with $B_{MIN} = 27$ nT/√Hz, for $n \sim 5 \times 10^{11}$ at 20 kHz [inset Fig. 4(b)]. The non-monotonic change of B_{MIN} is directly related to the nonlinearity of noise voltage [e.g., inset in Fig. 3(b)].

Finally, Fig. 4(c) shows the thermal stability of the molecular-doped Hall sensor through the temperature coefficient Δ_T, defined as the percentage change of R_H from its room temperature value per degree Celsius. Samples doped close to neutrality ($R_H = 1400$ Ω/T) display a temperature coefficient of $\Delta_T = -0.6\%/°C$ and undergo irreversible changes in the doping level at $T \approx 80$ °C (supplementary material S4). We achieve the highest thermal stability with samples annealed for ∼4 h at $T = 160$ °C, after which the room temperature R_H reached a stable value of $R_H \sim 300$ Ω/T due to partial desorption of dopants.[11] After this curing step at 160 °C, samples showed a fairly low $\Delta_T = -0.03\%/°C$ up to $T = 150$ °C, while still displaying respectable performance at $T = 150$ °C, with $S_V \sim 0.12$ V/(VT), $S_I \sim 300$ V/(AT), and $B_{MIN} \sim 100$ nT/√Hz.

Table I shows a comparison of our devices with other Hall sensors reported in the literature. The maximum current-related sensitivity in doped epigraphene is found to be on the order of $S_I \sim 1500$ V/(AT) at room temperature. This value is limited by the minimum n attained in our sample ($|n| < 5 \times 10^{11}$ cm^{-2}) and is set by the disorder present in the as-grown material, combined with additional contributions from external doping and thermally excited carriers in the dopant layer and the SiC substrate. Decoupling epigraphene and substrate by hydrogen intercalation has led to high μ at cryogenic temperatures. However, at room temperature, the lowest n values reported for H-intercalated epigraphene are all above 1×10^{12} cm^{-2}, with $\mu \sim 1300$–1700 cm^2/(V s).[40] These mobilities are lower than the highest reported for epigraphene at room temperature [$\mu = 5500$ cm^2/(V s)][23,41] and the ones achieved in this work [$\mu = 2300$ cm^2/(V s)]. Above room temperature, interactions between epigraphene and the substrate via longitudinal-acoustic and remote interfacial phonon scattering further degrade mobility. The stable temperature range ($T < 80$ °C) for samples doped close to the Dirac point is determined by our current choice of doping method.[11] A high thermal stability up to $T = 150$ °C is achieved after curing the samples at a temperature of 160 °C for 4 h. The resulting temperature coefficient $\Delta_T = -0.03\%/°C$ could then be understood as the intrinsic thermal drift of epigraphene and not due to desorption of dopants. This implies that by using an alternate thermally stable doping scheme, epigraphene could well outperform Hall element-based III–V at high temperatures.[29,36–38] Our work paves the way for the development of

TABLE I. Figures of merit for room temperature Hall sensor performance, including graphene-based Hall sensors and commercially available sensors based on silicon and III-V materials. Boldface denotes data from this work.

Type	S_I [V/(AT)]	S_V [V/(VT)]	B_{MIN} (nT/√Hz)	Frequency (kHz)
Si[29,35]	100	0.1	50–500	**0.1–100**
InSb[29,36–38]	140–700	1–7.2	1–60	0–50
GaAs[29,36–38]	30–3200	0.6–1	10–6000	0–50
hBN-G[12]	4100	2.6	50	3
CVD[15]	2093	0.35	100	3
CVD[13]	1200	N/A	300 000	3
CVD[14]	97	0.03	400 000	1
Epi[39]	1021	0.3	2000	3
Epi (this)	***1080***	***0.23***	***60, 40***	***3, 20***
Epi (this)	***1442***	***0.21***	***47, 27***	***3, 20***

epigraphene Hall sensors for real-world applications, which require durable, controllable, and sensitive devices produced in a scalable way.

See the supplementary material for extra data on sheet resistance vs carrier density, linearity error, offset voltage, and heating ramps.

We thank Alexander Tzalenchuk for insightful discussions. This work was jointly supported by the Swedish Foundation for Strategic Research (SSF) (Nos. GMT14-0077 and RMA15-0024), Chalmers Excellence Initiative Nano, VINNOVA (Nos. 2017-03604 and 2019-04426), and European Union's Horizon 2020 research and innovation programme under Marie Sklodowska-Curie Grant Agreement No 766025. This work was performed in part at Myfab Chalmers.

DATA AVAILABILITY

The authors declare that the main data supporting the findings of this study are available within this article and supplementary material. Additional data are available from the corresponding author upon request.

REFERENCES

[1]J. Heremans, J. Phys. D **26**, 1149 (1993).
[2]G. Boero, M. Demierre, P.-A. Besse, and R. S. Popovic, Sens. Actuators, A **106**, 314 (2003).
[3]P. Kejik, G. Boero, M. Demierre, and R. S. Popovic, Sens. Actuators, A **129**, 212 (2006).
[4]I. Shibasaki, J. Cryst. Growth **175-176**, 13 (1997).
[5]K. S. Novoselov, A. K. Geim, S. V. Morozov, D. Jiang, Y. Zhang, S. V. Dubonos, I. V. Grigorieva, and A. A. Firsov, Science **306**, 666 (2004).
[6]K. S. Novoselov, A. K. Geim, S. V. Morozov, D. Jiang, M. I. Katsnelson, I. V. Grigorieva, S. V. Dubonos, and A. A. Firsov, Nature **438**, 197 (2005).
[7]W. Zhu, V. Perebeinos, M. Freitag, and P. Avouris, Phys. Rev. B **80**, 235402 (2009).
[8]V. Cheianov and V. Fal'ko, Phys. Rev. Lett. **97**, 226801 (2006).
[9]J.-H. Chen, C. Jang, S. Adam, M. S. Fuhrer, E. D. Williams, and M. Ishigami, Nat. Phys. **4**, 377 (2008).
[10]J. Martin, N. Akerman, G. Ulbricht, T. Lohmann, J. H. Smet, K. von Klitzing, and A. Yacoby, Nat. Phys. **4**, 144 (2008).
[11]H. He, K. H. Kim, A. Danilov, D. Montemurro, L. Yu, Y. W. Park, F. Lombardi, T. Bauch, K. Moth-Poulsen, T. Iakimov, R. Yakimova, P. Malmberg, C. Müller, S. Kubatkin, and S. Lara-Avila, Nat. Commun. **9**, 3956 (2018).
[12]J. Dauber, A. A. Sagade, M. Oellers, K. Watanabe, T. Taniguchi, D. Neumaier, and C. Stampfer, Appl. Phys. Lett. **106**, 193501 (2015).
[13]C.-C. Tang, M.-Y. Li, L. J. Li, C. C. Chi, and J. C. Chen, Appl. Phys. Lett. **99**, 112107 (2011).
[14]A. Dankert, B. Karpiak, and S. P. Dash, Sci. Rep. **7**, 15231 (2017).
[15]L. Huang, Z. Zhang, B. Chen, X. Ma, H. Zhong, and L. M. Peng, Appl. Phys. Lett. **104**, 183106 (2014).
[16]J. Chan, A. Venugopal, A. Pirkle, S. McDonnell, D. Hinojos, C. W. Magnuson, R. S. Ruoff, L. Colombo, R. M. Wallace, and E. M. Vogel, ACS Nano **6**, 3224 (2012).
[17]C. Virojanadara, M. Syväjarvi, R. Yakimova, L. Johansson, A. Zakharov, and T. Balasubramanian, Phys. Rev. B **78**, 245403 (2008).
[18]K. v Emtsev, A. Bostwick, K. Horn, J. Jobst, G. L. Kellogg, L. Ley, J. L. McChesney, T. Ohta, S. A. Reshanov, J. Röhrl, E. Rotenberg, A. K. Schmid, D. Waldmann, H. B. Weber, and T. Seyller, Nat. Mater. **8**, 203 (2009).
[19]T. Ciuk, B. Stanczyk, K. Przyborowska, D. Czolak, A. Dobrowolski, J. Jagiello, W. Kaszub, M. Kozubal, R. Kozlowski, and P. Kaminski, IEEE Trans. Electron Devices **66**, 3134 (2019).
[20]K. H. Kim, S. Lara-Avila, H. He, H. Kang, Y. W. Park, R. Yakimova, and S. Kubatkin, Crystals **7**, 378 (2017).
[21]S. Kopylov, A. Tzalenchuk, S. Kubatkin, and V. I. Fal'Ko, Appl. Phys. Lett. **97**, 112109 (2010).
[22]A. Lartsev, T. Yager, T. Bergsten, A. Tzalenchuk, T. J. B. M. Janssen, R. Yakimova, S. Lara-Avila, and S. Kubatkin, Appl. Phys. Lett. **105**, 063106 (2014).
[23]S. Lara-Avila, K. Moth-Poulsen, R. Yakimova, T. Bjaßrnholm, V. Fal'Ko, A. Tzalenchuk, and S. Kubatkin, Adv. Mater. **23**, 878 (2011).
[24]H. He, S. Lara-Avila, K. H. Kim, N. Fletcher, S. Rozhko, T. Bergsten, G. Eklund, K. Cedergren, R. Yakimova, Y. W. Park, A. Tzalenchuk, and S. Kubatkin, Metrologia **56**, 045004 (2019).
[25]S. Lara-Avila, A. Danilov, D. Golubev, H. He, K. H. Kim, R. Yakimova, F. Lombardi, T. Bauch, S. Cherednichenko, and S. Kubatkin, Nat. Astron. **3**, 983 (2019).
[26]T. Yager, A. Lartsev, S. Mahashabde, S. Charpentier, D. Davidovikj, A. Danilov, R. Yakimova, V. Panchal, O. Kazakova, A. Tzalenchuk, S. Lara-Avila, and S. Kubatkin, Nano Lett. **13**, 4217 (2013).
[27]M. Cornils and O. Paul, in *Proceedings of the IEEE International Conference on Micro Electro Mechanical Systems (MEMS)* (IEEE, 2008), pp. 940–943.
[28]M. Cornils, *Sheet Resistance and Hall Mobility Determination Beyond Van Der Pauw* (Der Andere Verlag, 2009).
[29]R. S. Popović, *Hall Effect Devices* (Institute of Physics Publications, 2004).
[30]T. G. M. Kleinpenning, Sens. Actuators **4**, 3 (1983).
[31]M. A. Paun, J. M. Sallese, and M. Kayal, Sensors **13**, 2093 (2013).
[32]F. N. Hooge, Physica B+C **83**, 14 (1976).
[33]Y. Zhang, E. E. Mendez, and X. Du, ACS Nano **5**, 8124 (2011).
[34]S. Kim, H. Kim, and D. B. Janes, Jpn. J. Appl. Phys., Part 1 **50**, 102601 (2011).
[35]K. Vervaeke, E. Simoen, G. Borghs, and V. V. Moshchalkov, Rev. Sci. Instrum. **80**, 074701 (2009).
[36]Y. Sugiyama and S. Kataoka, Sens. Actuators **8**, 29 (1985).
[37]F. W. Bell, 2017 product catalog, https://fwbell.com/wp-content/uploads/2017/04/Hall-Generators-catalog-NEWER.pdf (2020).
[38]Akahi Kasei Microdevices, 2020 product catalog, https://www.akm.com/global/en/products/magnetic-sensor/ (2020).
[39]V. Panchal, K. Cedergren, R. Yakimova, A. Tzalenchuk, S. Kubatkin, and O. Kazakova, J. Appl. Phys. **111**, 07E509 (2012).
[40]E. Pallecchi, F. Lafont, V. Cavaliere, F. Schopfer, D. Mailly, W. Poirier, and A. Ouerghi, Sci. Rep. **4**, 4558 (2015).
[41]J. L. Tedesco, B. L. VanMil, R. L. Myers-Ward, J. M. McCrate, S. A. Kitt, P. M. Campbell, G. G. Jernigan, J. C. Culbertson, C. R. Eddy, and D. K. Gaskill, Appl. Phys. Lett. **95**, 122102 (2009).